

MIT Open Access Articles

Materials properties and dislocation dynamics in InAsP compositionally graded buffers on InP substrates

The MIT Faculty has made this article openly available. **Please share** how this access benefits you. Your story matters.

Citation: Jandl, Adam, Mayank T. Bulsara, and Eugene A. Fitzgerald. "Materials Properties and Dislocation Dynamics in InAsP Compositionally Graded Buffers on InP Substrates." *Journal of Applied Physics* 115, no. 15 (April 21, 2014): 153503. © 2014 AIP Publishing LLC.

As Published: <http://dx.doi.org/10.1063/1.4871289>

Publisher: American Institute of Physics

Persistent URL: <http://hdl.handle.net/1721.1/91951>

Version: Final published version: final published article, as it appeared in a journal, conference proceedings, or other formally published context

Terms of Use: Article is made available in accordance with the publisher's policy and may be subject to US copyright law. Please refer to the publisher's site for terms of use.



Materials properties and dislocation dynamics in InAsP compositionally graded buffers on InP substrates

Adam Jandl, Mayank T. Bulsara, and Eugene A. Fitzgerald

Citation: [Journal of Applied Physics](#) **115**, 153503 (2014); doi: 10.1063/1.4871289

View online: <http://dx.doi.org/10.1063/1.4871289>

View Table of Contents: <http://scitation.aip.org/content/aip/journal/jap/115/15?ver=pdfcov>

Published by the [AIP Publishing](#)

Articles you may be interested in

[Growth, microstructure, and luminescent properties of direct-bandgap InAlP on relaxed InGaAs on GaAs substrates](#)

[J. Appl. Phys.](#) **113**, 183518 (2013); 10.1063/1.4804264

[Relaxed, high-quality InP on GaAs by using InGaAs and InGaP graded buffers to avoid phase separation](#)

[J. Appl. Phys.](#) **102**, 033511 (2007); 10.1063/1.2764204

[Metamorphic InAs_yP_{1-y} \(y = 0.30 – 0.75\) and AlIn_{1-x}As_yP_{1-y} buffer layers on InP substrates](#)

[Appl. Phys. Lett.](#) **90**, 212113 (2007); 10.1063/1.2742649

[Carrier compensation and scattering mechanisms in Si-doped InAs_yP_{1-y} layers grown on InP substrates using intermediate InAs_yP_{1-y} step-graded buffers](#)

[J. Appl. Phys.](#) **100**, 063705 (2006); 10.1063/1.2349358

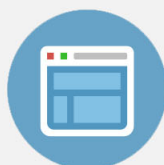
[Development of 6.00 Å graded metamorphic buffer layers and high performance In_{0.86}Al_{0.14}As_{1-x}In_{0.86}Ga_{0.14}As heterojunction bipolar transistor devices](#)

[J. Vac. Sci. Technol. B](#) **24**, 1492 (2006); 10.1116/1.2197516

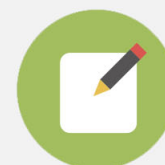


Re-register for Table of Content Alerts

Create a profile.



Sign up today!



Materials properties and dislocation dynamics in InAsP compositionally graded buffers on InP substrates

Adam Jandl,^{a)} Mayank T. Bulsara, and Eugene A. Fitzgerald
*Department of Materials Science and Engineering, Massachusetts Institute of Technology,
 77 Massachusetts Ave. Cambridge, Massachusetts 02139, USA*

(Received 6 February 2014; accepted 2 April 2014; published online 16 April 2014)

The properties of InAs_xP_{1-x} compositionally graded buffers grown by metal organic chemical vapor deposition are investigated. We report the effects of strain gradient (ϵ /thickness), growth temperature, and strain initiation sequence (gradual or abrupt strain introduction) on threading dislocation density, surface roughness, epi-layer relaxation, and tilt. We find that gradual introduction of strain causes increased dislocation densities ($>10^6/\text{cm}^2$) and tilt of the epi-layer ($>0.1^\circ$). A method of abrupt strain initiation is proposed which can result in dislocation densities as low as $1.01 \times 10^5 \text{ cm}^{-2}$ for films graded from the InP lattice constant to InAs_{0.15}P_{0.85}. A model for a two-energy level dislocation nucleation system is proposed based on our results. © 2014 AIP Publishing LLC. [<http://dx.doi.org/10.1063/1.4871289>]

I. INTRODUCTION

Compositionally graded buffers of various alloys have allowed for low defect density lattice-mismatched devices to be integrated on a variety of substrates.¹⁻⁴ In the past decade, research on InAs_xP_{1-x} graded buffers has provided for the development of thermophotovoltaics, infrared photodetectors, and high-speed electronics on InP.⁵⁻⁷ These applications rely on the low band gap and high electron mobility of In_yGa_{1-y}As alloys latticed matched to various compositions of InAs_xP_{1-x}. Since the lattice constants of the In_yGa_{1-y}As compositions of interest are not matched to any binary alloy substrates, InAs_xP_{1-x} graded buffers are used to create low defect density virtual substrates for the In_yGa_{1-y}As device structures. Other alloy choices which span the same range of lattice constants are In_yGa_{1-y}As or In_zAl_{1-z}As. However, both of these alloys suffer from issues of phase separation (resulting from the solution of In with Ga or Al on the group-III sub-lattice) which make it more difficult to fabricate the high quality buffers required.⁸ InAs_xP_{1-x} does not phase separate since it is a mixed group-V alloy. In this article, we document the development of high quality InAs_xP_{1-x} compositionally graded buffers grown by metal-organic chemical vapor deposition (MOCVD).

While many previous studies have employed InAs_xP_{1-x} graded buffers, only a few have discussed the quality and defect densities produced by these structures.^{5,8} We present a discussion and detailed analysis of the relaxation process in InAs_xP_{1-x} linearly graded buffers on InP. Our results show evidence of asymmetric relaxation in the low arsenic ($x < 0.2$), initial layers of the graded buffer and suggest a dislocation nucleation process which must be avoided to achieve a low defect density structure. We show that the way strain is introduced during the initial graded buffer steps plays a critical role in the final threading dislocations density (TDD). We propose a method to promote the nucleation of

dispersed threading dislocations. We show that this method results in lower TDD and surface roughness of the final graded buffer cap layer.

II. METHODS

A. Growth

Epitaxial growth was done in a Thomas-Swan close-coupled showerhead metal-MOCVD reactor. Chemical reactants were trimethyl-indium, arsine, and phosphine. The group V to group III reactant (V/III) ratio was 160 or 320. The substrates were semi-insulating (001) on-axis InP purchased from AXT, Inc. All growths were conducted with N₂ carrier gas as the ambient at a growth pressure of 100 Torr. All epitaxial processes began with a 500 nm homoepitaxial InP layer. Two methods of compositional grading were used. In linearly graded buffers, the InAs_xP_{1-x} composition was continually graded from InP towards InAs by computer-controlled reactant flow changes. In step-graded buffers, the composition was incremented in 2%As steps and the thickness of these layers determined the average strain gradient (SG). The strain gradient for all structures was approximately 0.5% strain/ μm (except where noted otherwise). The final layer in the structure was a 1 μm layer of InAs_xP_{1-x} with a composition matching the last layer in the graded buffer. This capping layer makes the observation of threading dislocations in plan-view transmission electron microscopy (TEM) easier since it prevents misfit dislocations from obscuring the field of view. The growth time of the cap layer also provides additional time for the underlying film to relax. Cooling from the growth temperature to 350 °C was done under an overpressure of arsine and phosphine to prevent any degradation of the sample surface due to the evaporation of the group V species.

Table I provides a summary of the experiments and the parameters of each sample used in the studies. Three sets of experiments were implemented to determine the effects of

^{a)}Author to whom correspondence should be addressed. Electronic mail: jandl@mit.edu

TABLE I. Growth and experimental parameters of the InAs_xP_{1-x} Compositionally Graded Buffers.

Study	Growth temperature (°C)	Strain gradient (% ϵ /μm)	Grading method	Initial misfit (%)	Cap composition (%As)	V/III	TDD (#/cm ²)	RMS surface roughness 5 × 5 μm / 25 × 25 μm (nm)
SG	650	0.53	Linear	0.0	37	160	3.29 × 10 ⁶	2.4 / 4.84
SG	650	0.33	Linear	0.0	44	160	1.63 × 10 ⁶	0.3 / 4.81
SG ^a	650	0.41	Linear	0.0	39	160	2.95 × 10 ⁶	1.0 / 4.26
SG	650	1.37	Linear	0.0	38	160	5.9 × 10 ⁶	1.7 / 5.22
SG	650	0.0	39	160	7.34 × 10 ⁸	35.4 / 36.7
Temp., SI ^b	650	0.55	Step	0.0	16	160	3.33 × 10 ⁶	1.4 / 3.8
Temp.	675	0.48	Step	0.0	14	320	1.30 × 10 ⁶	0.5 / 4.3
Temp.	700	0.48	Step	0.0	14	320	7.20 × 10 ⁵	0.6 / 3.8
SI	650	0.51	Step	0.16	15	160	1.27 × 10 ⁵	0.6 / 3.2
SI	650	0.55	Step	0.34	16	160	1.01 × 10 ⁵	0.3 / 1.7
SI	650	0.55	Step	0.53	16	160	1.88 × 10 ⁶	0.4 / 1.9

^aSG: strain gradient.^bSI: strain initiation.

growth temperature (Temp), SG, and strain initiation (SI) sequence on threading dislocation density, nucleation, and surface roughness. Each experimental set consisted of graded buffers grown with the variation of one design parameter. At growth temperatures of 650 °C, a V/III ratio of 160 was used, but at temperatures above 650 °C a greater V/III ratio of 320 was used. The greater V/III ratio at higher temperatures was needed to compensate for the increase in the phosphorus vapor pressure with temperature. Growth rates for all temperatures were between 0.35 and 0.54 nm/s. For the growth temperature experimental set, the growth temperatures ranged from 650 °C to 700 °C in 25 °C increments and the graded buffers were step graded to 15 %As. For the strain gradient experiments, the composition was linearly graded from 0 %As to 40 %As while the thickness of the graded buffer was adjusted to vary the strain gradient between 0.33 %strain/μm to 1.37 %strain/μm. In the strain initiation experiments, the misfit of the initial layer was varied between 0.16 % (5 %As) and 0.51 % (15 %As). The thickness of this initial layer was such that all structures had the same final thickness. After the initiation layer, the structures were step graded to 15 %As. All structures in the strain gradient and strain initiation experimental sets were grown at 650 °C.

B. Analysis

Samples in these experiments were analyzed by TEM, high resolution x-ray diffraction (HRXRD), and atomic force microscopy (AFM) to measure the material properties (lattice constant, composition, residual strain, crystallographic tilt, dislocation density, and surface roughness) and experimental variables (thickness and lattice mismatch to InP).

Cross-sectional TEM (XTEM) was used to measure the layer thicknesses and plan-view TEM (PVTEM) was used to measure the threading dislocations density (#/cm²) by directly counting the dislocations in a minimum of thirty five (35) randomly selected fields of view (a total minimum of 690 μm²) of the final epilayer. The 95 % confidence intervals for the threading dislocation density measurements were calculated using the sample standard deviation of the dislocation population from the PVTEM images and Student's T

distribution. It should be noted that XTEM cannot provide an accurate value for the TDD since only a very small area of the sample is observed compared to the observable areas in PVTEM. TEM samples were prepared by manual mechanical grinding and polishing followed by Ar⁺ ion milling. Since the films contain indium, it was necessary to use two milling steps at 3 kV and 2 kV or less. The latter step helps to remove the indium rich droplets that form during the former step. Images were collected with a JEOL 2011 microscope operating at 200 kV.

A relationship between the threading dislocation density, strain rate, and dislocation glide velocity has been previously reported by Fitzgerald *et al.* and Yang *et al.*^{2,3,9,10} Their theory predicts the number of threading dislocations which must be nucleated in a graded buffer for a constant growth rate, strain gradient, and glide velocity. Since the growth rate and strain gradient are both experimental parameters, a proportionality between the dislocation density and glide velocity is given by

$$\rho = \frac{2C_f g_r}{bv}, \quad (1)$$

where ρ is the threading dislocation density, C_f is the strain gradient, g_r is the growth rate, and v is the dislocation glide velocity. The in-plane Burgers vector is represented by b and is equivalent to $0.707a$ (a being the relaxed lattice constant). Glide velocity is a temperature dependent quantity, so Eq. (1) can be written as

$$\rho = \frac{2C_f g_r}{bv_o \left(\frac{\sigma_{eff}}{\sigma_o} \right)^m e^{\frac{-E_a}{k_b T}}}, \quad (2)$$

where v_o is a constant prefactor, m is a power factor which depends on the material system, σ_{eff} is the effective shear stress acting on the dislocations, σ_o is a constant to remove the stress dimensions from the equation, E_a is the activation energy for nucleation glide, k_b is Boltzmann's constant, and T is the temperature.

Symmetric (004) and asymmetric (224) HRXRD reciprocal space maps (RSM) were used to calculate the composition

and residual strain in the cap layers and the crystallographic tilt which may have developed during the growth of the graded buffer. A Bruker D8 diffractometer using radiation from the Cu $K_{\alpha 1}$ transition and a linear array detector were used to create the RSMs. To calculate the strain in the [100] and [010] directions, two sets of RSMs were collected with the (110) and (1 $\bar{1}$ 0) diffraction planes, respectively. The reciprocal space coordinates in this paper are defined such that

$$\begin{aligned} q_x^{(004)} &= 0 \text{ \AA}^{-1} \\ q_z^{(004)} &= \frac{40}{a_{(001)}} \text{ \AA}^{-1}, \end{aligned} \quad (3)$$

where $a_{(001)}$ is plane spacing between the (001) planes, which will be denoted as a_3 , and is the plane spacing for the planes nearly perpendicular to the wafer's surface normal direction (neglecting the change in orientation due to epi-layer tilt or unintentional miscut of the substrate). Additionally, a_1 and a_2 will indicate the plane spacing of the (100) and (010) planes as determined by the reciprocal lattice maps along the [1 $\bar{1}$ 0] or [110] directions.

Correction of the position of the reciprocal lattice points (RLP) due to tilt and substrate mis-alignment (due to any unintentional offcut or goniometer configuration) followed the methods of Roesener *et al.*¹¹ Tilt of the epilayers, γ , was determined directly from the RSMs by

$$\tan(\gamma) = \frac{\Delta q_x^{(004)}}{\frac{20}{a_s} - |\Delta q_z^{(004)}|}, \quad (4)$$

where a_s is the relaxed lattice constant of the substrate and Δq_i is the difference in between the film peak and substrate peak for the referenced coordinate. The observed epilayer RLP could then be corrected to the true RLP by a rotation of the observed RLP (but not the substrate RLP) about the origin through the angle γ . The true lattice constants of the epi-layers could then be determined from the tilt corrected RLP by (all further references to the q_x and q_z coordinates assumes the tilt corrections)

$$\begin{aligned} a_{1,2} &= a_s \left(1 - \frac{\Delta q_x^{(224)}}{\frac{20\sqrt{2}}{a_s} + \Delta q_x^{(224)}} \right) \\ a_3 &= a_s \left(1 - \frac{\Delta q_z^{(004)}}{\frac{40}{a_s} + \Delta q_z^{(004)}} \right). \end{aligned} \quad (5)$$

These measurements and methods of tilt corrections were performed independently for the RSMs collected along the [1 $\bar{1}$ 0] or [110] directions.

Once the lattice constants are known, three independent strains can be determined by

$$\varepsilon_i = \frac{a_R - a_i}{a_R}; \quad i = 1, 2, 3. \quad (6)$$

By using Hooke's law under plane stress conditions, $\sigma_3 = 0$, the relaxed lattice constant, a_R , can be found with

$$a_R = \frac{c_{11}}{c_{11} + 2c_{12}} a_3 + \frac{c_{12}}{c_{11} + 2c_{12}} (a_1 + a_2) \quad (7)$$

and the elastic constants, c_{ij} , are determined by the epi-layer properties. The relaxation of the epi-layer is then defined as

$$R_i = \frac{a_i - a_s}{a_R - a_s}; \quad i = 1, 2. \quad (8)$$

The average relaxation of the epi-layer can be calculated as the geometric average of the relaxations found in Eq. (8) as shown by Roesener *et al.* (Ref. 11)

$$\bar{R} = \frac{1}{2} (R_1 + R_2). \quad (9)$$

A Nanoscope IV AFM measured the root-mean-square (RMS) roughness of the samples. Two scan sizes were used, $5 \times 5 \mu\text{m}$ and $25 \times 25 \mu\text{m}$. The former can image the bunching of atomic steps at the surface while the latter images the cross-hatch morphology. The cross-hatch morphology is a result of dislocation pile-ups, which create deep trenches, or the strain fields emanating from the misfit arrays in the graded buffer, which create small amplitude ripples.^{2,12}

III. RESULTS

Figures 1 and 2 show typical XTEM images of linear and step graded buffers, respectively. XTEM imaging used either the $\langle 110 \rangle$ pole condition (not pictured) or the bright field $\langle 220 \rangle$ two-beam condition. The former is the proper alignment for thickness measurements, while the latter gives improved contrast to the dislocations in the structure. XTEM micrographs were used to confirm the layer thickness of the cap and entire graded layer. The average strain gradient was calculated once the cap composition was measured by HRXRD.

HRXRD RSMs of linearly graded buffers revealed distinctive features of $\text{InAs}_x\text{P}_{1-x}$ buffers. Figure 3 shows a typical RSM for these structures. The map shows that tilt (Eq. (4)) initially develops in the graded buffer but is abruptly halted

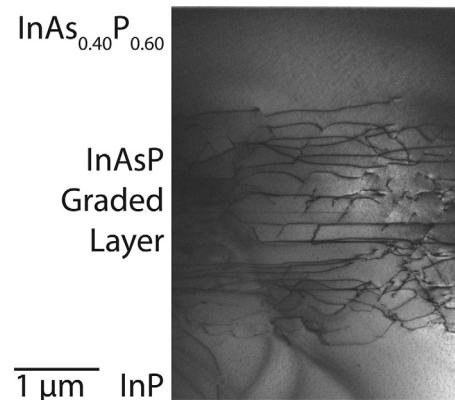


FIG. 1. Typical cross-sectional TEM micrograph of a linearly graded $\text{InAs}_x\text{P}_{1-x}$ buffer imaged with the 220 two-beam diffraction condition. The thin dark lines running nearly horizontal are misfit dislocations. No threading dislocations are observed in the cap layer. The image was edited with non-linear brightness and contrast layers in addition to sharpening effects to enhance the visibility of the dislocations.

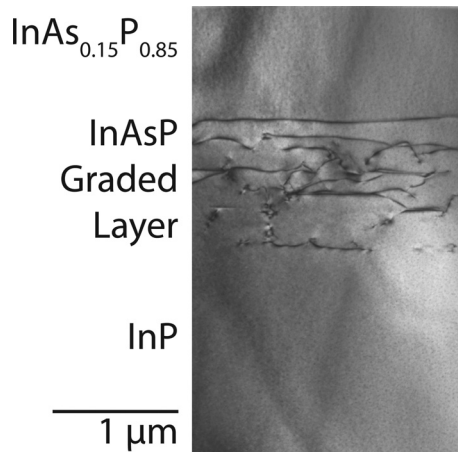


FIG. 2. Typical cross section TEM micrograph of a step graded $\text{InAs}_x\text{P}_{1-x}$ buffer imaged with the bright-field 220 two-beam diffraction condition. The thin dark lines running nearly horizontal are misfit dislocations.

when the composition reaches 15–20%As. Tilt is often observed in graded buffers and results from an imbalanced population of the type of Burgers vectors possessed by the misfit dislocations.¹³ Since the nature of the tilt changed, it implies a dislocation nucleation event occurred which changed the balance of the dislocation population.

The threading dislocation density and surface roughness were measured for samples grown at temperatures between 650 °C and 700 °C. The purpose of these experiments was to determine how dislocation nucleation and glide were affected by the growth temperature. As the temperature was increased from 650 °C, the threading dislocation density decreased toward a minimum at 700 °C (Figure 4). Equation (2) was fit (with $C_f = 0.4\%$ strain/ μm , $g_r = 0.4\text{ nm/s}$, and a equal to the InP lattice constant) to the data to determine the activation energy for dislocation glide. This energy was found to be 1.3 eV. The surfaces of all samples were slightly roughened due to the formation of cross-hatch morphology or dislocation pile-ups (Figure 5).

Figure 6 shows the threading dislocation density of the strain initiation experimental set. The dislocation density

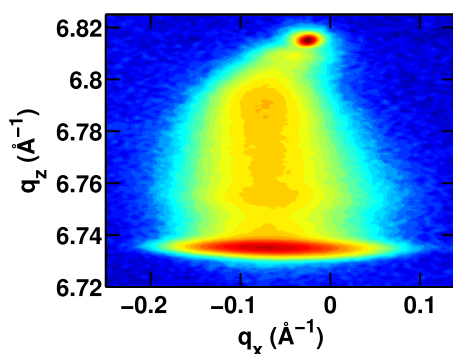


FIG. 3. HRXRD RSM of the symmetric 004 reciprocal lattice point of a typical, linearly graded, $\text{InAs}_x\text{P}_{1-x}$ buffer. The small peak at the top of the figure is the InP substrate and the broader peak at the bottom of the figure is the $\text{InAs}_{0.36}\text{P}_{0.64}$ cap. The intensity between these peaks was diffracted by the graded buffer layer. In the initial layers of the graded buffer tilt (Eq. (4)) develops in the negative q_x direction but abruptly stops developing when the composition is between 15–20%As. The color scale is logarithmic.

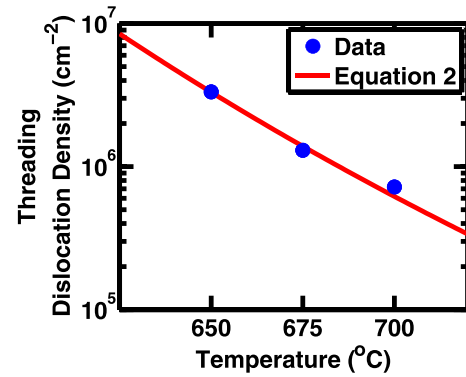


FIG. 4. The threading dislocation density as a function of the growth temperature was measured by PVTEM. Increasing the temperature from 650 °C to 700 °C decreased the threading dislocation density by about one order of magnitude. The V/III ratio was 160 at 650 °C and 320 for temperatures of 675 °C and above. The 95 % confidence intervals fall within the markers for the data. Equation (4) is fit to the data with $E_a = 1.3\text{ eV}$ which is slightly lower than the values reported for InP and InAs by Yonenaga *et al.*¹⁴

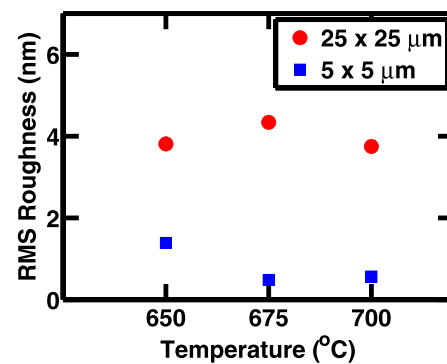


FIG. 5. AFM measurements of the root mean square surface roughness for structures with different growth temperatures. The V/III ratio was 160 at 650 °C and 320 for temperatures of 675 °C and above.

decreased by more than an order of magnitude when a strain initiation layer of either 5 or 10 %As was used (0.16 % and 0.34 % misfit, respectively). When the initial misfit was increased, to 15 %As (0.53 % misfit), the dislocation density increased to an amount similar to the graded buffer which did not have abruptly initiated strain. The surface roughness

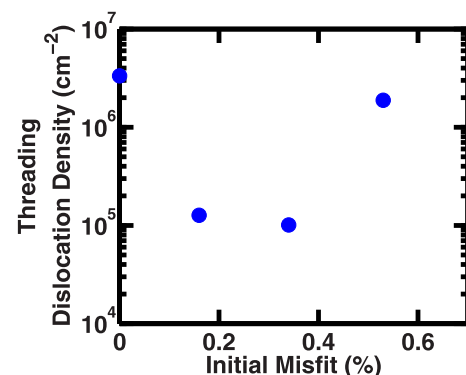


FIG. 6. The threading dislocation density in the cap layer for the three structures which had abruptly initiated strain and for one structure which was step graded from 0 %As (plotted as having 0 % initial misfit). The 95 % confidence intervals fall within the markers for the data.

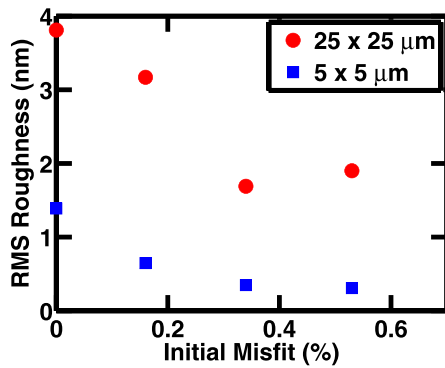


FIG. 7. AFM measurements of the root mean square surface roughness for various initial misfits. For the 0% initial misfit sample, the composition was step graded from the InP lattice constant without an abrupt strain layer. The legend indicates the dimensions of the measured region.

(Figure 7) did not follow the same trend; however, the minimum surface roughness was still observed when the initial misfit was 0.53%. The roughness for all structures which had abrupt strain initiation was lower than for the structure which had gradual strain initiation. Although the differences in surface roughness were not large, the trend implied that the mechanism of surface roughening was reduced by the abrupt strain initiation.

HRXRD of the strain initiation experimental set indicated a difference in the dislocation nucleation and relaxation process of the abruptly initiated graded buffers. Figure 8 shows the RSMs of the four structures included in the strain initiation experimental set and the absolute value of the tilt (Eq. (4)) of the cap layer which was measured from the RSMs. Together, these plots show that the tilt decreased as the initial misfit increased. The reduction in tilt suggested that the population of Burgers vectors which were created during the dislocation process were becoming more evenly distributed between the eight (8) possible glissile orientations allowed in a compressively strained film. Additionally, Figure 9 shows that the average relaxation in the cap layers increased with the initial misfit. This

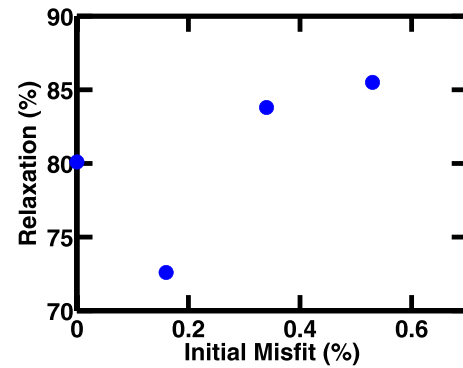


FIG. 9. The average relaxation as a function of the initial misfit in the graded buffer. HRXRD measured the relaxation in two perpendicular $\langle 100 \rangle$ directions and the average relaxation was calculated with Eq. (9). For the 0% initial misfit sample, the composition was step graded from the InP lattice constant without an abrupt strain layer.

implied that there was less impediment to the glide of the threading dislocations during the relaxation of these structures.

By measuring the threading dislocation density as a function of the strain gradient, the average glide velocity could be estimated. Plotting Eq. (1) with glide velocities of 0.1 – 0.8 $\mu\text{m/s}$ ($C_f = 0.4\% \text{ strain}/\mu\text{m}$, $g_r = 0.4 \text{ nm/s}$, and a equal to the InP lattice constant) shows an appropriate range of values (Figure 10). A sample which intentionally lacked a graded buffer was used for a comparison. All the samples were grown at 650 °C to a final composition of approximately $\text{InAs}_{0.4}\text{P}_{0.6}$ confirmed by HRXRD. The thickness of the graded buffers was measured with XTEM. The thickness and composition allowed for the strain gradient to be calculated.

IV. DISCUSSION

Fitting Eq. (2) to the experimental data in Figure 4 allowed us to determine the activation energy of 1.3 eV for glide in the $\text{InAs}_x\text{P}_{1-x}$ material system. This value is slightly lower than the activation energies reported by Yonenaga for

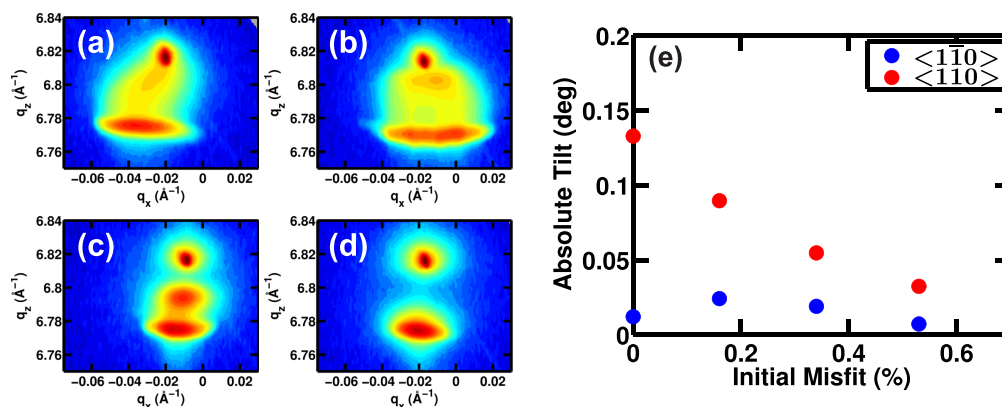


FIG. 8. (a) RSM with a $\langle 110 \rangle$ diffraction plane of a step graded $\text{InAs}_x\text{P}_{1-x}$ buffer. (b)–(d) RSMs with a $\langle 110 \rangle$ diffraction plane of step graded buffers with abrupt strain initiation. The additional peak observed between the cap layer and substrate layer in (b) and (c) can be used to calculate the lattice constant and composition of the initiation layer. The structure measured in (d) was intentionally initiated at the same composition as the cap, so the initiation and cap layers are contained in the same peak. (e) The absolute value of the tilt (Eq. (4)) of the cap layer for the 4 structures measured in (a)–(d). The tilt values for (a) are plotted as having 0% initial misfit. The crystallographic directions indicated in the legend refer to the diffraction plane normal used during the collection of the RSMs. Tilt was recorded as defined by Ref. 11.

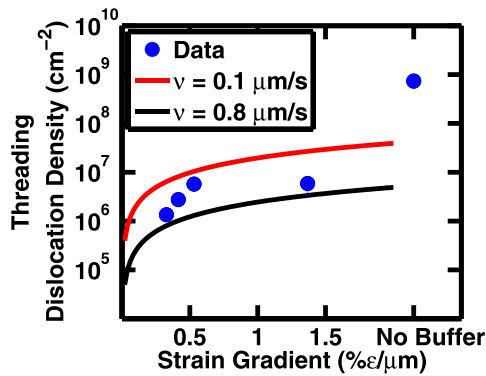


FIG. 10. Experimental data and theoretical fit of graded buffers with different strain gradients. The error bars are 95% confidence intervals and fall inside the markers for most of the data points. Equation (1) is plotted with two glide velocities, as noted in the legend. The sample labeled “No Buffer” intentionally lacked any graded buffer and was used as a point of comparison. This point was not included in the dataset when fitting.

α and β dislocations in InP and InAs.¹⁴ Since the values for v_o or the stress factors are not individually known, but are constant given a constant strain rate, only the product can be fit. This stress adjusted velocity factor should be of order $10^5 - 10^6$ cm/s as shown by Fitzgerald *et al.* (who estimated that the Young’s Modulus is of order 10^5 MPa, and ϵ_{eff} is of order 10^{-4} for a SiGe compositionally graded system, but the same values are applicable to the $\text{InAs}_x\text{P}_{1-x}$ system) but was determined to be of order 10 cm/s.¹⁰ This reduction in glide velocity is a result of reduced effective stress caused by an impediment to dislocation motion.¹⁰ The most probable cause of the reduced glide velocities is dislocation pile-ups which would also explain the increased surface roughness (Figure 5) observed in these structures.

Equation (1) can explain the results in Figure 10 and again suggests that dislocation glide is being restricted. A fit of the data is not reasonable, since the dependence of the effective stress on the strain gradient is unknown. Instead, a range of glide velocities can be plotted to bound the estimate of v . The range of appropriate glide velocities is $0.1 - 0.8 \mu\text{m/s}$. This range was less than the glide velocities for $\text{GaAs}_w\text{Sb}_{1-w}$ reported by Yang *et al.* (Ref. 3), and InP or InAs reported by Yonenaga *et al.* (Refs. 15 and 16). These lower glide velocities indicate that the dislocation motion was being impeded, and was again prescribed to the presence of dislocation pile-ups. Since the formation of pile-ups depends on the dislocation nucleation process, we considered the nucleation process in greater detail.

From the HRXRD RSMs (Figure 3) of the linearly graded buffer, there appeared to be two stages of dislocation nucleation. Initially, the graded buffer developed tilt which indicated that the Burgers vectors were not equally distributed between the eight possible glissile orientations. The structure continued to tilt until the composition was between 15 and 20 %As. At this point, tilt stopped developing which suggested a sudden nucleation event had occurred to balance the population of Burgers vectors among the possible orientations. Since the orientation of the existing Burgers vectors could not have been redistributed nor eliminated, the total number of dislocations in the structure must have increased

by a large amount to make the original imbalance of orientations insignificant. A two energy level model for the dislocation nucleation process was created to explain the observations of initial epilayer tilt, two stage nucleation, and reduced dislocation glide velocities. In the model, there are two types of sites (corresponding to the two nucleation events), one with low activation energy and density (#/area) of nucleation sites and the second has a higher activation energy and density (Figure 11). Before continuing with a discussion of the results, a brief explanation of this hypothesis is provided.

Since a majority of the film area may lack the lower activation energy sites, the model can be explained as consisting of three phase of relaxation of $\text{InAs}_x\text{P}_{1-x}$ graded buffers: strain initiation, primary nucleation, and secondary nucleation. During the strain initiation phase (shown left of the grey, dashed line in Figures 11(a) and 11(b)), the strain energy in the film is below the activation energy for nucleation so the strain energy continues to increase as a function of both the thickness and increasing misfit. Once the strain energy reaches the lower activation energy (the red line in Figure 11), the primary nucleation phase begins but only at a

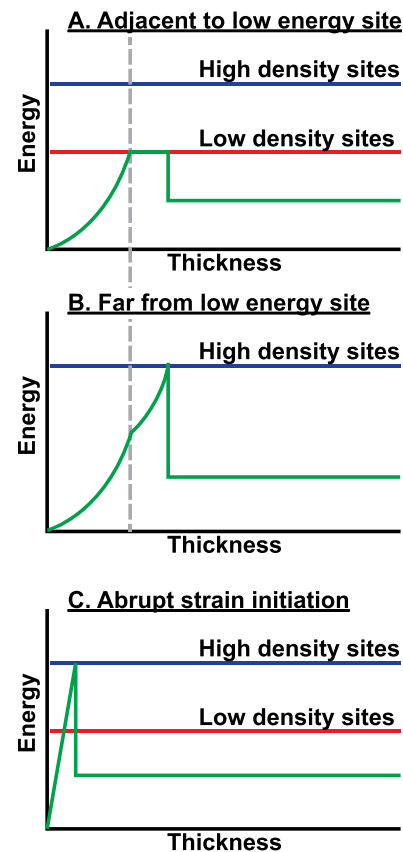


FIG. 11. Schematic diagram showing the strain and activation energies as a function of thickness for three proposed situations during the growth and relaxation of $\text{InAs}_x\text{P}_{1-x}$ graded buffers. Red and blue lines indicate the relative activation energies of the two nucleation sites discussed in the text. The green curve represents the strain energy of the film during growth. Parts (a) and (b) occur simultaneously during growth when strain is gradually introduced in the graded buffer. Part (c) occurs only during abrupt strain initiation. The key feature of the abrupt initiation sequence is the activation of both low and high energy activation sites allowing for a more uniform dislocation population.

few sites throughout the film area. Dislocations which are nucleated from regions similar to Figure 11(a) will then glide away from the low density nucleation sites towards the regions similar to Figure 11(b), which cannot yet nucleate dislocations. These later regions continue to experience an increase in the strain energy but at a lower rate. This phase is pictured as just to the right of the grey, dashed line in Figure 11 and continues until the sharp drop of the strain energy. The final phase of secondary nucleation begins when the strain energy in regions with only high activation energy sites are able to begin nucleation. At this point, the entire film can relax at the same rate and the steady-state implied by Eq. (2) is established.

The consequences of this three phase nucleation process can explain the lower glide velocities, tilt, surface roughness, and RSMs observed in the linearly graded buffers. Since nucleation from the low energy sites is likely to be from particles or wafer edges, the dislocations are likely to have the same Burgers vector and be aligned along a few $\langle 110 \rangle$ directions (Refs. 17–19) which could lead to tilt of the epi-layers, surface roughness and lower glide velocities from dislocation pile-ups (Ref. 12).

If nucleation from the sites with a higher density could be promoted over the low density sites, then it is possible that a more spatially uniform distribution of dislocations would be created (Figure 11(c)). This reduces the probability for dislocation interactions and ultimately reduces the threading dislocation density. The strategy to nucleate a more uniform population of dislocations, that we investigated here, has been employed previously by Vineis *et al.* but has not been discussed in the literature.²⁰ Erdtmann *et al.* have shown how an initially greater density of dislocations can allow for faster strain gradients and lower threading dislocation densities in the final film.²¹

To promote nucleation from the higher activation energy sites, we increased the rate at which strain energy accumulates in the initial phase. In these experiments, we grew a constant composition layer directly on the substrate. The goal was to rapidly raise the strain energy above the higher activation energy and site density level. While such a high strain energy would allow for nucleation from both the low and high density sites, it may still favor the high density sites. Since dislocations nucleated at the low density sites would be highly localized, they would require some amount of time to glide and relax the film. Therefore, regions far from the low energy sites would be able to nucleate dislocations from the high energy sites earlier. Since this would lower the strain energy in a majority of the film area, nucleation would only be active for a short time. Once dislocations are present in the film, any amount of additional strain can be relaxed by glide of the dislocations. The dislocations nucleated at the higher energy level are likely to be created at surface steps which means that they are unlikely to have the same Burgers vectors or glide planes.²² This should substantially reduce the formation of dislocation pile-ups and epi-layer tilt. Ideally, the population of dislocations nucleated would be controlled to a number just sufficient to relax the film given a strain gradient and growth rate (Eq. (2)).

By initiating layers with increased misfit, the final threading dislocation density was reduced. Figure 6 shows that having an initial misfit of either 0.16% or 0.34% decreased the dislocation density by about an order of magnitude compared to the other structures in the same set. Additionally, structures which had abrupt strain initiation had decreased surface roughness (Figure 7), decreased tilt (Figure 8), and increased relaxation of the cap layer (Figure 9) compared to the structure which had gradually initiated strain. These results suggest that there is no favored orientation of Burgers vectors and dislocation pile-ups are not created and therefore do not interrupt the glide of threading dislocations. Additionally, we conclude that nucleation of dislocations in the $\text{InAs}_x\text{P}_{1-x}$ abruptly initiated graded buffers follows a process similar to Figure 11(c) as opposed to the processes of Figures 11(a) and 11(b).

V. CONCLUSION

We have investigated the relaxation and dislocation nucleation processes in $\text{InAs}_x\text{P}_{1-x}$ compositionally graded buffers. The results show that gradually initiated strain in the graded buffer layers leads to the development of tilt and eventually a large dislocation nucleation event. Reduced dislocation densities, tilt, and surface roughness as well as increased relaxation can be achieved by initiating the graded buffer layer with a strained layer as high as 0.34%. The initial strain in this layer promotes the nucleation of dislocations throughout the epi-layer and prevents the formation of dislocation pile-ups. Additionally, favorable results were obtained at higher growth temperatures. These results show that the $\text{InAs}_x\text{P}_{1-x}$ material system provides a low defect density platform for the development of minority carrier devices.

ACKNOWLEDGMENTS

This work was supported as part of the Solid State Solar Thermal Energy Conversion Center, an Energy Frontier Research Center funded by the U.S. Department of Energy, Office of Science, Basic Energy Sciences under Award No. DE-FG02-09ER46577. This work made use of the MRSEC Shared Experimental Facilities at MIT, supported by the National Science Foundation under Award No. DMR-08-19762.

¹E. A. Fitzgerald, Y. H. Xie, M. L. Green, D. Brasen, A. R. Kortan, J. Michel, Y. J. Mii, and B. E. Weir, *Appl. Phys. Lett.* **59**, 811 (1991).

²E. A. Fitzgerald, Y. H. Xie, D. Monroe, P. J. Silverman, J. M. Kuo, A. R. Kortan, F. A. Thiel, and B. E. Weir, *J. Vac. Sci. Technol. B* **10**, 1807 (1992).

³L. Yang, M. T. Bulsara, K. E. Lee, and E. A. Fitzgerald, *J. Cryst. Growth* **324**, 103 (2011).

⁴A. Y. Kim, W. S. McCullough, and E. A. Fitzgerald, *J. Vac. Sci. Technol. B* **17**, 1485 (1999).

⁵M. K. Hudait, Y. Lin, D. M. Wilt, J. S. Speck, C. A. Tivarus, E. R. Heller, J. P. Pelz, and S. A. Ringel, *Appl. Phys. Lett.* **82**, 3212 (2003).

⁶C. A. Wang, E. K. Duerr, J. P. Donnelly, D. R. Calawa, and D. C. Chapman, *J. Cryst. Growth* **310**, 1583 (2008).

⁷M. K. Hudait, Y. Lin, M. N. Palmisiano, and S. A. Ringel, *IEEE Electron Device Lett.* **24**, 538 (2003).

- ⁸M. K. Hudait, Y. Lin, M. N. Palmisiano, C. Tivarus, J. P. Petz, and S. A. Ringel, *J. Appl. Phys.* **95**, 3952 (2004).
- ⁹E. A. Fitzgerald, *Mater. Sci. Rep.* **7**, 87 (1991).
- ¹⁰E. A. Fitzgerald, A. Y. Kim, M. T. Currie, T. A. Langdo, G. Taraschi, and M. T. Bulsara, *Mater. Sci. Eng., B* **67**, 53 (1999).
- ¹¹T. Roesener, V. Klinger, C. Weuffen, D. Lackner, and F. Dimroth, *J. Cryst. Growth* **368**, 21 (2013).
- ¹²S. B. Samavedam and E. A. Fitzgerald, *J. Appl. Phys.* **81**, 3108 (1997).
- ¹³J. A. Olsen, E. L. Hu, S. R. Lee, I. J. Fritz, A. J. Howard, B. E. Hammons, and J. Y. Tsao, *J. Appl. Phys.* **79**, 3578 (1996).
- ¹⁴I. Yonenaga, *Mater. Trans.* **46**, 1979 (2005).
- ¹⁵I. Yonenaga, *J. Appl. Phys.* **84**, 4209 (1998).
- ¹⁶I. Yonenaga and K. Sumino, *Appl. Phys. Lett.* **58**, 48 (1991).
- ¹⁷M. F. Ashby and L. Johnson, *Philos. Mag.* **20**, 1009 (1969).
- ¹⁸C. J. Gibbings, C. G. Tuppen, and M. Hockly, *Appl. Phys. Lett.* **54**, 148 (1989).
- ¹⁹P. Feichtinger, M. S. Goorsky, D. Oster, T. D'Silva, and J. Moreland, *J. Electrochem. Soc.* **148**, G379 (2001).
- ²⁰C. Vineis, V. Yang, M. Currie, R. Westhoff, and C. Leitz, "Methods of fabricating semiconductor heterostructures," US7368308 B206-May-2008.
- ²¹M. Erdtmann, M. T. Currie, J. C. Woicik, and D. Black, *MRS Proc.* **891**, 0891-EE12-05 (2005).
- ²²B. Pichaud, N. Burle, M. Texier, C. Alfonso, M. Gailhanou, J. Thibault-Pénisson, C. Fontaine, and V. I. Vdovin, *Phys. Status Solidi C* **6**, 1827 (2009).